Volume 20 | Number 45 | 7 December 2018 | Pages 7223–7402

CrystEngComm

rsc.li/crystengcomm

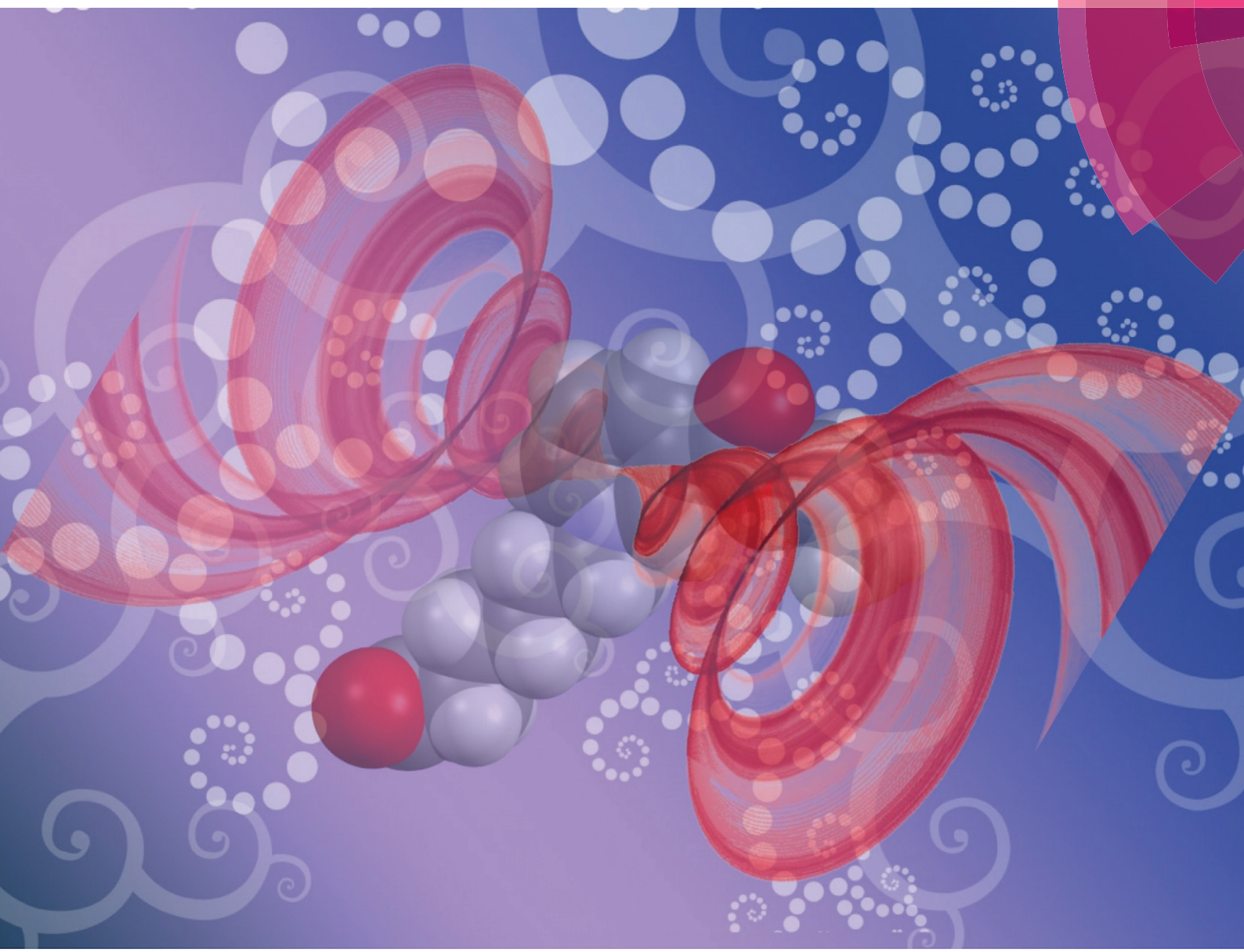

ROYAL SOCIETY OF CHEMISTRY

PAPER

Kwang-Ming Lee *et al.*

Anion-controlled supramolecular crystal structures and ionic liquids from fatty acid-substituted ethyl-nicotinate ionic compounds

CrystEngComm

PAPER

View Article Online
View Journal | View Issue

Cite this: *CrystEngComm*, 2018, **20**, 7248

Anion-controlled supramolecular crystal structures and ionic liquids from fatty acid-substituted ethyl-nicotinate ionic compounds†

Wei-Jie Chang, Padi Yi-Syong Su and Kwang-Ming Lee *

Received 14th May 2018,
Accepted 19th September 2018

DOI: 10.1039/c8ce00785c

rsc.li/crystengcomm

A series of bio-inspired fatty acid-substituted ethyl-nicotinate ionic compounds, 1-(5-carboxypentyl)-3-(ethoxycarbonyl)pyridin-1-ium ionic compounds ([Nia-OEt-C5COOH] X, X = Br^- (**1**), $B(Ph)_4^-$ (**2**), NO_3^- (**3**), BF_4^- (**4**), PF_6^- (**5**), and OTf^- (**6**)) were synthesized. The supramolecular crystal structures of **1** and **2** were characterized by single crystal X-ray diffraction. The Nia-OEt-C5COOH cations in the two crystal structures formed dimerized secondary rectangular motifs with weak C–H…O═C hydrogen bonding which extended into a lipid-like bilayer and a β-sheet-like tape stacking, respectively. Four acidic ionic liquids (AILs) were formed by the other anions (**3**–**6**) because these anions and the two carbonyl O atoms of the Nia-OEt-C5COOH cation have small hydrogen bonding acceptor ability differences. In addition, the flexible ester group of Nia-OEt-C5COOH has a low barrier to the rotation of the C–O–C bonds, making it less rigid and it has a lower melting point. The four AILs were characterized by DSC thermal analysis, infrared spectroscopy and ionic conductivity.

Introduction

Molecular design is a fascinating field, developing methodologies to gain desired solid and liquid materials such as crystal structures and ionic liquids (ILs) for specific applications and investigations.[1–16] Among the methodologies which attempt to control the crystal or liquid states of ionic target compounds, one such method involves the use of flexible or rotatable functional groups. Because these groups are sometimes able to disturb the optimal intermolecular interactions between cationic moieties and anions and result in ionic liquids rather than solids. Here we report the synthesis of a series of fatty acid-substituted ethyl-nicotinate ionic compounds with distinct anions ([Nia-OEt-C5COOH] X, X = Br^- (**1**), $B(Ph)_4^-$ (**2**), NO_3^- (**3**), BF_4^- (**4**), PF_6^- (**5**), and OTf^- (**6**)). This study is based on our previous report on a series of hydrogen-bonded biomimetic dimerized rectangular secondary structure motifs formed by fatty acid-substituted nicotinamide salts,[17] which highlighted the roles of C–H…X (X = N, O, π and anions) hydrogen bonding because the C–H could replace the N–H as the hydrogen-bonding donor to form similar rectangular secondary structure motifs. The initial motivation of this study was to investigate whether rectangular secondary structure motifs could be formed when the planar nicotinamide was changed to ethyl-nicotinate which has a rotatable ethyl acetate group. The results show that the Br^- (**1**) and $B(Ph)_4^-$ (**2**) salts are solids with a C–H–O hydrogen bonded secondary rectangular motif, however, the NO_3^- (**3**), BF_4^- (**4**), PF_6^- (**5**), and OTf^- (**6**) ionic compounds are ILs at room temperature. These four ILs can be classified as being acidic ionic liquids (AILs). AILs have attracted much attention and have been used in a wide range of applications involving electrochemistry, catalysis, CO_2 fixation, membranes and pharmaceutics.[18] AILs possess acidic properties and retain the typical characteristics of ILs. A large number of functionalized sulfate groups in cations or anions have been reported in AILs, but carboxylic acids are rare.[8]

Experimental

General procedures

^{1}H NMR spectra were recorded with an Agilent DD2-400 instrument. Samples were dissolved in DMSO and tetramethylsilane was used as an internal standard. Elemental analyses were carried out with an Elementar vario EL III instrument. DSC measurements were performed, under a nitrogen atmosphere, with a TA Instruments DSC Q200 instrument. Indium was used as the standard for temperature calibration. The samples (~3 mg) were encapsulated in sealed aluminum pans. Single-crystal data collection was carried out with a Bruker SMART APEX II diffractometer equipped with a SMART CCD array detector with graphite monochromatized Mo-K_α radiation (λ = 0.71073 Å) in the ϕ

Department of Chemistry, National Kaohsiung Normal University, 62 Shen-Shung Road, Kaohsiung 82444, Taiwan. E-mail: kmlee@nknu.edu.tw

† Electronic supplementary information (ESI) available. CCDC 1533668 (for **1**) and 1533667 (for **2**). For ESI and crystallographic data in CIF or other electronic format see DOI: 10.1039/c8ce00785c

and ω scan modes. All the structures were solved and refined by the full-matrix least-squares method (based on F^2 using all independent data) using the SHELXS-97 and SHELXL-97 programs.[19] Ionic conductivity measurements were carried out under air using an impedance analyzer (Electrochemical Analyzer model 600C series). The ionic conductivities were measured using comb-shaped gold electrodes, as reported by Kato *et al.*[20]

General materials and methods

All chemical reagents and solvents were obtained from commercial sources and used without purification. All reactions were carried out under a nitrogen atmosphere in anhydrous solvents. The 1-(5-carboxypentyl)-3-(ethoxycarbonyl)pyridin-1-ium bromide salt **1** was synthesized first by the reaction of ethyl 3-pyridinecarboxylate with 6-bromohexanoic acid. The $B(Ph)_4^-$ (**2**), NO_3^- (**3**), BF_4^- (**4**), PF_6^- (**5**), and OTf^- (**6**) ionic compounds were prepared *via* the reaction of salt **1** with $NaB(Ph)_4$ and silver salts (AgX, X = NO_3^-, BF_4^-, PF_6^-, and OTf^- salts, respectively). The synthetic pathways of these compounds are shown in Scheme 2.

1-(5-Carboxypentyl)-3-(ethoxycarbonyl)pyridin-1-ium bromide salt 1

A solution of ethyl nicotinate (5.03 g, 33.30 mmol) and 6-bromohexanoic acid (6.35 g, 32.58 mmol) was refluxed in acetonitrile (40 mL) for 72 h and then allowed to cool to room temperature. A yellow liquid was obtained, and the solvent was removed in a rotary evaporator. The resultant crude product was recrystallized from ethanol/diethyl ether to give product **1** as a white solid with a yield of 66%. Needle-shaped crystals suitable for single-crystal X-ray diffraction were obtained by the slow diffusion of diethyl ether into the ethanol solution. ^{1}H-NMR (400 MHz, d^6-DMSO, δ/ppm): 12.03 (s, 1H, –O*H*), 9.63 (s, 1H, –N–C*H*), 9.31 (d, 1H, J = 6.3 Hz, –N–C*H*), 8.98 (d, 1H, J = 11.0 Hz, –N–CH–CH–C*H*), 8.29 (dd, 1H, J = 8.2, 6.3 Hz, –N–CH–CH–C*H*), 4.71 (t, 2H, J = 7.4 Hz, –N–CH_2), 4.45 (q, 2H, J = 7.3 Hz, –O–CH_2–CH$_3$), 2.22 (t, 2H, J = 7.2 Hz, –CO–CH_2), 1.94 (quin, 2H, J = 7.6 Hz, –CO–CH$_2$–CH_2), 1.54 (quin, 2H, J = 7.4 Hz, –N–CH–C*H*), 1.38 (t, 3H, J = 7.2 Hz, –O–CH$_2$–CH_3), 1.31 (quin, 2H, J = 7.6 Hz, –N–CH–CH–C*H*). ^{13}C NMR (100 MHz, d^6-DMSO, δ/ppm): 174.48 (C═O-acid), 162.13 (C═O-ester), 148.32 (*o*-py), 146.41 (*p*-py), 145.51 (*o*-py), 130.59 (*m*-py), 128.80 (*m*-py), 63.05 (CH$_2$-fatty acid), 61.24 (CH$_2$-ester), 33.28 (CH$_2$-fatty acid), 30,70 (CH$_2$-fatty acid), 21.27 (CH$_2$-fatty acid), 14.44 (CH$_3$-eter). Elemental analysis calcd (%) for $C_{14}H_{20}BrNO_4$: C, 48.15; H, 5.91; N, 4.04. Found: C, 48.57; H, 5.82; N, 4.05.

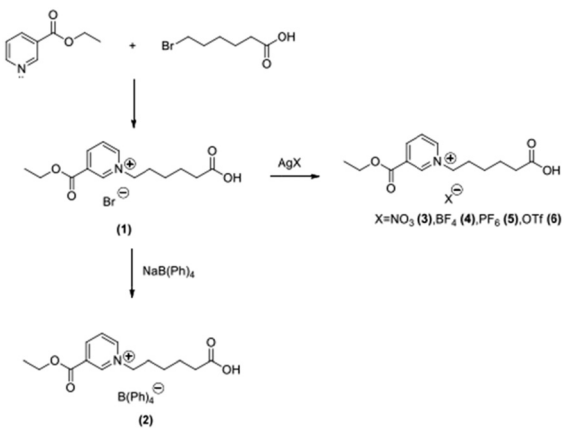

Scheme 1 Synthetic pathways of ethyl nicotinate cation with different anions.

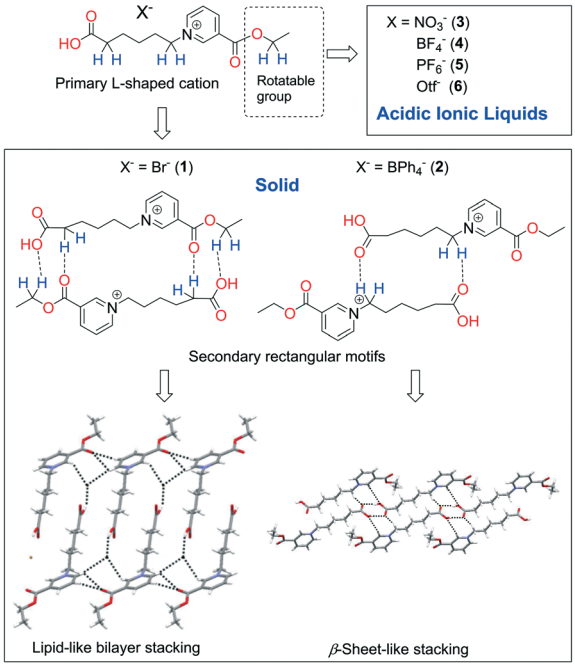

Scheme 2 Ethyl nicotinate cations serve as a building block to form secondary rectangular motifs and consequently to construct a lipid-like bilayer and a β-sheet-like stacking for Br^- (**1**) and $B(Ph)_4^-$ (**2**) respectively. The different anions used to obtain ionic liquid compounds for NO_3^- (**3**), BF_4^- (**4**), PF_6^- (**5**), and OTf^- (**6**) due to the disturbance of the rotatable ethoxyl group.

1-(5-Carboxypentyl)-3-(ethoxycarbonyl)pyridin-1-ium tetraphenylborate (2)

A solution of bromide salt **1** (1.00 g, 2.90 mmol) in deionized water (15 mL) was added to a 15 mL aqueous solution of $NaB(Ph)_4$ (1.02 g, 2.96 mmol) at room temperature to give a yellow-green precipitate. The solid was filtered and washed with deionized water to remove NaBr. Then, the yellow-green powder **2** was collected with a yield of 96%. Block-shaped crystals suitable for single-crystal X-ray diffraction were obtained by the slow diffusion of diethyl ether into the acetonitrile solution. ^{1}H-NMR (400 MHz, d^6-DMSO, δ/ppm): 12.02 (s, 1H, –O*H*), 9.62 (s, 1H, –N–C*H*), 9.26 (d, 1H, J = 5.9 Hz, –N–C*H*), 8.97 (d, 1H, J = 8.2 Hz, –N–CH–CH–C*H*), 8.26 (t, 1H, J = 8.0 Hz, –N–CH–CH–C*H*), 7.10–7.22 (m, 8H), 6.91 (t, 8H, J = 7.4 Hz), 6.77 (t, 8H, J = 7.2 Hz), 4.68 (t, 2H, J = 7.4 Hz, –N–CH_2), 4.44 (q, 2H, J = 7.0 Hz, –O–CH_2–CH$_3$), 2.21 (t, 2H, J =

7.2 Hz, –CO–CH_2), 1.93 (quin, 2H, J = 7.0 Hz, –CO–CH$_2$–CH_2), 1.53 (quin, 2H, J = 7.4 Hz, –N–CH–CH), 1.37 (t, 3H, J = 7.2 Hz, –O–CH$_2$–CH_3), 1.30 (quin, 2H, J = 7.6 Hz, –N–CH–CH–CH). ^{13}C NMR (100 MHz, d^6-DMSO, δ/ppm): 174.52 (C═O-acid), 163.56 (q, J = 49.5, *ipso*-BPh$_4$), 162.11 C═O-ester), 148.26 (*o*-py), 146.41 (*p*-py), 145.49 (*o*-py), 135.97 (*o*-BPh$_4$), 130.60 (*m*-py), 128.78 (*m*-py), 125.72 (*m*-BPh$_4$), 121.95 (*p*-BPh$_4$), 63.06 (CH$_2$-fatty acid), 61.27 (CH$_2$-ester), 33.34 (CH$_2$-fatty acid), 30.71 (CH$_2$-fatty acid), 21.30 (CH$_2$-fatty acid), 12.43 (CH$_3$-eter). Elemental analysis calcd (%) for $C_{38}H_{40}BNO_4$: C, 77.95; H, 6.89; N, 2.39. Found: C, 76.47; H, 7.02; N 2.37.

1-(5-Carboxypentyl)-3-(ethoxycarbonyl)pyridin-1-ium nitrate (3)

A solution of bromide salt **1** (1.00 g, 2.90 mmol) in deionized water (15 mL) was added to a 15 mL aqueous solution of $AgNO_3$ (0.51 g, 3.00 mmol) at room temperature in the dark, and a yellow-green precipitate of AgBr was observed. The AgBr precipitate was filtered and the filtrate was collected. The solvent was then removed by rotary evaporation to obtain a transparent liquid. The crude product was purified by dissolving with ethanol and then precipitating with diethyl ether to remove excess AgBr. The solution was filtered, and the solvent was removed by rotary evaporation. Finally, the liquid was washed with ethanol several times until no AgBr precipitated. A transparent liquid was obtained with a yield of 26%. ^{1}H-NMR (400 MHz, d^6-DMSO, δ/ppm): 12.03 (br, 1H, –OH), 9.61 (s, 1H, –N–CH), 9.28 (d, 1H, J = 6.3 Hz, –N–CH), 8.96 (d, 1H, J = 8.2 Hz, –N–CH–CH–CH), 8.27 (dd, 1H, J = 8.0, 6.1 Hz, –N–CH–CH–CH), 4.69 (t, 2H, J = 7.4 Hz, –N–CH_2), 4.43 (q, 2H, J = 7.0 Hz, –O–CH_2–CH$_3$), 2.21 (t, 2H, J = 7.2 Hz, –CO–CH_2), 1.93 (quin, 2H, J = 7.6 Hz, –CO–CH$_2$–CH_2), 1.53 (quin, 2H, J = 7.5 Hz, –N–CH–CH), 1.37 (t, 3H, J = 7.2 Hz, –O–CH$_2$–CH_3), 1.30 (quin, 2H, J = 7.6 Hz, –N–CH–CH–CH). ^{13}C NMR (100 MHz, d^6-DMSO, δ/ppm): 174.50 (C═O-acid), 162.11 (C═O-ester), 148.28 (*o*-py), 146.39 (*p*-py), 145.50 (*o*-py), 130.59 (*m*-py), 128.80 (*m*-py), 63.06 (CH$_2$-fatty acid), 61.30 (CH$_2$-ester), 33.31 (CH$_2$-fatty acid), 30,69 (CH$_2$-fatty acid), 21.30 (CH$_2$-fatty acid), 14.43 (CH$_3$-eter). Elemental analysis calcd (%) for $C_{14}H_{20}N_2O_7$: C, 51.22; H, 6.14; N 8.53. Found: C, 51.32; H, 6.01; N. 8.43.

1-(5-Carboxypentyl)-3-(ethoxycarbonyl)pyridin-1-ium tetrafluoroborate (4)

A solution of bromide salt **1** (0.51 g, 1.48 mmol) in deionized water (15 mL) was added to a 15 mL aqueous solution of $AgBF_4$ (0.30 g, 1.52 mmol) at room temperature in the dark, and a yellow-green precipitate of AgBr was observed. The AgBr precipitate was filtered and the filtrate was collected. The solvent was then removed by rotary evaporation to obtain a transparent liquid. The crude product was purified by dissolving with ethanol and then precipitating with diethyl ether to remove excess AgBr. The solution was filtered, and the solvent was removed by rotary evaporation. Finally, the liquid was washed with ethanol several times until no AgBr precipitated. A transparent liquid was obtained with a yield of 50%. ^{1}H-NMR (400 MHz, d^6-DMSO, δ/ppm): 12.01 (br, 1H, –OH), 9.61 (s, 1H, –N–CH), 9.26 (d, 1H, J = 5.9 Hz, –N–CH), 8.95–8.98 (m, 1H, –N–CH–CH–CH), 8.26 (dd, 1H, J = 8.0, 6.1 Hz, –N–CH–CH–CH), 4.68 (t, 2H, J = 7.4 Hz, –N–CH_2), 4.44 (q, 2H, J = 7.0 Hz, –O–CH_2–CH$_3$), 2.21 (t, 2H, J = 7.2 Hz, –CO–CH_2), 1.93 (quin, 2H, J = 7.6 Hz, –CO–CH$_2$–CH_2), 1.53 (quin, 2H, J = 7.4 Hz, –N–CH–CH), 1.37 (t, 2H, J = 7.2 Hz, –O–CH$_2$–CH_3), 1.30 (quin, 2H, J = 7.6 Hz, –N–CH–CH–CH). ^{13}C NMR (100 MHz, d^6-DMSO, δ/ppm): 174.51 (C═O-acid), 162.12 (C═O-ester), 148.29 (*o*-py), 146.40 (*p*-py), 145.51 (*o*-py), 130.60 (*m*-py), 128.79 (*m*-py), 63.05 (CH$_2$-fatty acid), 61.28 (CH$_2$-ester), 33.29 (CH$_2$-fatty acid), 30,70 (CH$_2$-fatty acid), 21.29 (CH$_2$-fatty acid), 14.44 (CH$_3$-eter). Elemental analysis calcd (%) for $C_{16}H_{20}BF_4NO_5$: C, 45.31; H, 5.97; N 3.77. Found: C, 45.09; H, 6.23; N, 3.75.

1-(5-Carboxypentyl)-3-(ethoxycarbonyl)pyridin-1-ium hexafluorophosphate (5)

A solution of bromide salt **1** (0.31 g, 0.90 mmol) in deionized water (15 mL) was added to a 15 mL aqueous solution of $AgPF_6$ (0.25 g, 1.0 mmol) at room temperature in the dark, and a yellow-green precipitate of AgBr was observed. The AgBr precipitate was filtered and the filtrate was collected. The solvent was then removed by rotary evaporation to obtain a transparent liquid. The crude product was purified by dissolving with ethanol and then precipitating with diethyl ether to remove excess AgBr. The solution was filtered and the solvent was removed by rotary evaporation. Finally, the liquid was washed with ethanol several times until no AgBr precipitated. A transparent liquid was obtained with a yield of 50%. ^{1}H-NMR (400 MHz, d^6-DMSO, δ/ppm): 12.01 (br, 1H, –OH), 9.62 (s, 1H, –N–CH), 9.27 (d, 1H, J = 5.9 Hz, –N–CH), 8.97 (d, 1H, J = 8.2 Hz, –N–CH–CH–CH), 8.27 (dd, 1H, J = 8.0, 6.1 Hz, –N–CH–CH–CH), 4.68 (t, 2H, J = 7.6 Hz, –N–CH_2), 4.44 (q, 2H, J = 7.0 Hz, –O–CH_2–CH$_3$), 2.21 (t, 2H, J = 7.2 Hz, –CO–CH_2), 1.93 (quin, 2H, J = 7.6 Hz, –CO–CH$_2$–CH_2), 1.53 (quin, 2H, J = 7.4 Hz, –N–CH–CH), 1.37 (t, 2H, J = 7.0 Hz, –O–CH$_2$–CH_3), 1.30 (quin, 2H, J = 7.5 Hz, –N–CH–CH–CH). ^{13}C NMR (100 MHz, d^6-DMSO, δ/ppm): 174.49 (C═O-acid), 162.13 (C═O-ester), 148.27 (*o*-py), 146.41 (*p*-py), 145.50 (*o*-py), 130.61 (*m*-py), 128.79 (*m*-py), 63.06 (CH$_2$-fatty acid), 61.29 (CH$_2$-ester), 33.01 (CH$_2$-fatty acid), 30,71 (CH$_2$-fatty acid), 21.28 (CH$_2$-fatty acid), 14.42 (CH$_3$-eter). Elemental analysis calcd (%) for $C_{14}H_{20}F_6NO_4P$: C, 40.88; H, 4.90; N 3.41. Found: C, 40.94; H, 5.11; N, 3.31.

1-(5-Carboxypentyl)-3-(ethoxycarbonyl)pyridin-1-ium trifluoromethanesulfonate (6)

A solution of bromide salt **1** (1.01 g, 2.93 mmol) in deionized water (15 mL) was added to a 15 mL aqueous solution of AgOTf (0.77 g, 3.01 mmol) at room temperature in the dark, and a yellow-green precipitate of AgBr was observed. The AgBr precipitate was filtered and the filtrate was collected. The solvent was then removed by rotary evaporation to obtain

a transparent liquid. The crude product was purified by dissolving with ethanol and then precipitating with diethyl ether to remove excess AgBr. The solution was filtered and the solvent was removed by rotary evaporation. Finally, the liquid was washed with ethanol several times until no AgBr precipitated. A transparent liquid was obtained with a yield of 60%. ^{1}H-NMR (400 MHz, d^6-DMSO, δ/ppm): 12.02 (br, 1H, –O*H*), 9.62 (s, 1H, –N–C*H*), 9.27 (d, 1H, J = 5.9 Hz, –N–C*H*), 8.97 (d, 1H, J = 8.2 Hz, –N–CH–CH–C*H*), 8.27 (dd, 1H, J = 8.0, 6.1 Hz, –N–CH–CH–C*H*), 4.68 (t, 2H, J = 7.6 Hz, –N–CH_2), 4.44 (t, 2H, J = 7.0 Hz, –O–CH_2–CH$_3$), 2.21 (t, 2H, J = 7.2 Hz, –CO–CH_2), 1.93 (quin, 2H, J = 7.6 Hz, –CO–CH$_2$–CH_2), 1.53 (quin, 2H, J = 7.4 Hz, –N–CH–C*H*), 1.37 (t, 2H, J = 7.2 Hz, –O–CH$_2$–CH_3), 1.30 (quin, 2H, J = 7.7 Hz, –N–CH–CH–C*H*). ^{13}C NMR (100 MHz, d^6-DMSO, δ/ppm): 174.48 (C═O-acid), 162.11 (C═O-ester), 148.30 (*o*-py), 146.40 (*p*-py), 145.51 (*o*-py), 130.58 (*m*-py), 128.80 (*m*-py), 120.81 (q, CF$_3$S) 63.05 (CH$_2$-fatty acid), 61.27 (CH$_2$-ester), 33.28 (CH$_2$-fatty acid), 30,70 (CH$_2$-fatty acid), 21.27 (CH$_2$-fatty acid), 14.43 (CH$_3$-eter). Elemental analysis calcd (%) for C$_{15}$H$_{20}$F$_3$NO$_7$S·2H$_2$O: C, 39.91; H, 5.36; N, 3.10; S, 7.10. Found: C, 40.03; H, 5.78; N, 3.11; S, 6.97.

Results and discussion

1-(5-carboxypentyl)-3-(ethoxycarbonyl)pyridin-1-ium ionic compounds with distinct anions, Br$^-$ (**1**), B(Ph)$_4^-$ (**2**), NO$_3^-$ (**3**), BF$_4^-$ (**4**), PF$_6^-$ (**5**), and OTf$^-$ (**6**), were investigated (Scheme 1). The Br$^-$ (**1**) and B(Ph)$_4^-$ (**2**) salts were obtained as single crystals. The detailed crystal data are listed in Tables S1 and S2, and Fig. S1 and S2.† Scheme 2 shows that the ethyl nicotinate cations and fatty acid groups of **1** and **2** can form a well-defined rectangular secondary structure motif with C–H…O═C hydrogen bonding. The remaining four ionic compounds (NO$_3^-$ (**3**), BF$_4^-$ (**4**), PF$_6^-$ (**5**), and OTf$^-$ (**6**)) were investigated by thermal analysis, FT-IR spectrum and ionic conduction.

In the crystal of the Br$^-$ salt (**1**), the cationic moieties of the 1-(5-carboxypentyl)-3-(ethoxycarbonyl)pyridin-1-ium exhibit linear structures that hydrogen bond to each other in a head-to-tail manner to form centrosymmetric dimerized rectangular motifs (Fig. 1a) consisting of the two linear cations with the weak hydrogen bonded to each other of C7–H7A…O4═C14 (2.545 Å) and C13–H13B…O1═C6 (2.742 Å). A similar result was previously reported for the betaine-ester analogues of 1-*N*-alkyl-3-*N*″-methyl imidazolium salts [C$_1$, EC$_{16}$–Im]Br.[21] The C–H…Br and C–H…O hydrogen bonding leads the molecular stacking to form layered structures (Fig. 1b). The two kinds of molecular stacking are discussed in terms of hydrogen-bonding interaction. In the paired cations, one is the catemer due to the oxygen of the ester group and the hydrogen of the pyridine ring. Another is the dimerized rectangular structure produced by the oxygen of the carboxylic group and hydrogen of the ethyl ester group. Furthermore, there is a π–π interaction between the two cations *via* the two pyridine rings (π–π interaction distance of 3.385 Å) (Fig. 1c). For the anion, Br$^-$ is a strong hydrogen bond acceptor anion and is located between the pyridinium cations and acid group to form five hydrogen bonds: one strong O–H…Br

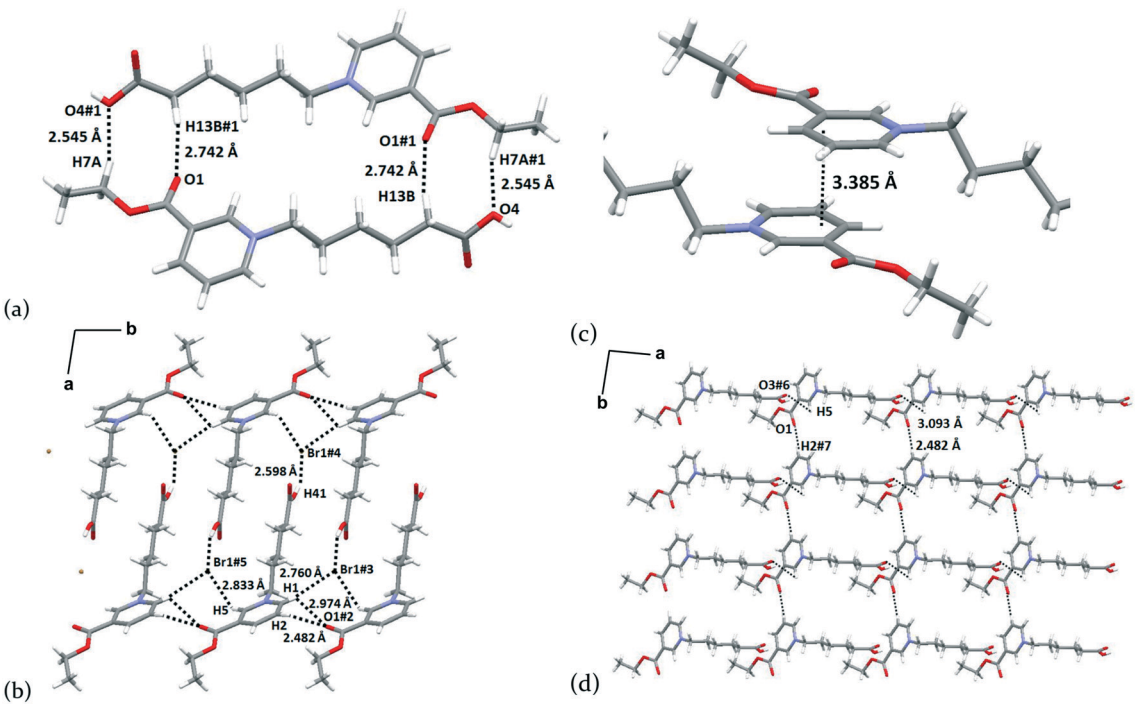

Fig. 1 The hydrogen-bonding motif and packing of the Br$^-$ salt (**1**). (a) The rectangular building block. (b) The layer stacking arrangement with cations surrounding the Br$^-$ anions. (c) The formation of π–π interactions by two cations of the pyridinium ring. (d) The 2-D network-supramolecular assembled *via* nonconventional hydrogen bonds.

hydrogen bond and four weak C–H…Br hydrogen bonds (Fig. 1b). The weak hydrogen bonds are formed *via* the ring hydrogens of the pyridinium cations and the hydrogens of the carbon closest to the oxygen of the ester group, respectively. This is because of the increased proton donor ability of the C–H moiety due to the charging of the pyridinium ring and the higher electronegativity of oxygen. Finally, the two-dimensional (2D) hydrogen bonding network consists of the weak hydrogen bonds C5-H5…O3═C14 (3.093 Å) and C2–H2…O1═C6 (2.482 Å). For $B(Ph)_4^-$ salt (2), the dimerized rectangular motifs consist of the two L-shaped cations connected by the weak hydrogen bonds O6–H16…O4═C11 2.609 Å (Fig. 2a). Furthermore, the weak C–H…O hydrogen bonds of the $B(Ph)_4^-$ anions form one-dimensional belt structures with the strong hydrogen bond O–H…O and the weak hydrogen bond C–H…O for cations. First, the dimeric construction of the carboxylic acids R-COOH involves intermolecular bonding *via* an O–H…O hydrogen bridge (O2–H2…O4═C11 1.784 Å) and a C–H…O hydrogen bond (C5–H17…O2–C11 2.922 Å). Then, the dimerized rectangular structure is produced by the hydrogen bond between the C═O group of the carboxylic acid and the hydrogen of the α-CH_2 group (O6–H16…O4═C11 2.609 Å) (Fig. 2b). Finally, there is a weak C–H…O hydrogen bond involving the –CH– group of benzene for the $B(Ph)_4^-$ and carbonyl groups of the ester functionality. Moreover, many C–H…π interactions can be formed, both between cations and anions and between anions. The BPh_4^- anions located between the cations and four benzene rings (R1–R4 in Fig. 2c) of each BPh_4^- anion form six weak C–H…π interactions with the adjacent cations, including two C_{ring}–H…π (C13–H5…R1 and C12–H6…R2) and four C–H…π (C1–H1…R2, C6–H15…R3, C6–H16…R3, and C6–H15…R4) interactions, as shown in Fig. 2c. C–H…π interactions have been previously reported in similar results using BPh_4^- salt.[22,23]

From the quite different molecular conformations and packing structures of the Br^- and BPh_4^- salts it can be deduced that their hydrogen bonding acceptor abilities play a vital role. As shown in Fig. 1 and 2, there are four hydrogen bonding acceptors in the two crystal systems: Br^-, two carbonyl O atoms (carboxylic acid and ester groups) and BPh_4^- which are listed in order from strong to weak hydrogen bonding acceptor abilities. As a result, the Br^- anions dominate the hydrogen bonding system in the Br^- salt, nevertheless, the carbonyl O atoms (carboxylic acid and ester groups) dominate the hydrogen bonding system in the BPh_4^- salt. This description can be supported by the formation of COOH…X hydrogen bonding because the carboxylic acid H atom is the stronger hydrogen bonding donor in the two crystal system. As we have seen in Fig. 1 and 2, COOH…Br^- and carboxylic acid dimers were formed in Br^- and BPh_4^- salts respectively. However, the preference is not only to bond to the strongest hydrogen bonding donor, the strongest acceptors also form the maximum number of hydrogen bonds with the C–H donors of pyridinium rings and α-CH_2 groups. For this reason, in salt **1**, the Br^- anions located between the pyridinium cations and acid group form five hydrogen bonds (one strong O–H…Br hydrogen bond and four weak C–H…Br hydrogen bonds) resulting in a lipid-type bilayer packing (Fig. 1b). Alternatively, in salt **2**, the carbonyl O atoms of the acid and ester groups bond to the C–H donors of the pyridinium rings and the α-CH_2 groups to form the maximum number of hydrogen bonds, thus, a β-sheet-like tape structure was formed. For ILs **3–6**, we suggest that the hydrogen bonding acceptor abilities and rotatable ethoxyl groups could explain why they

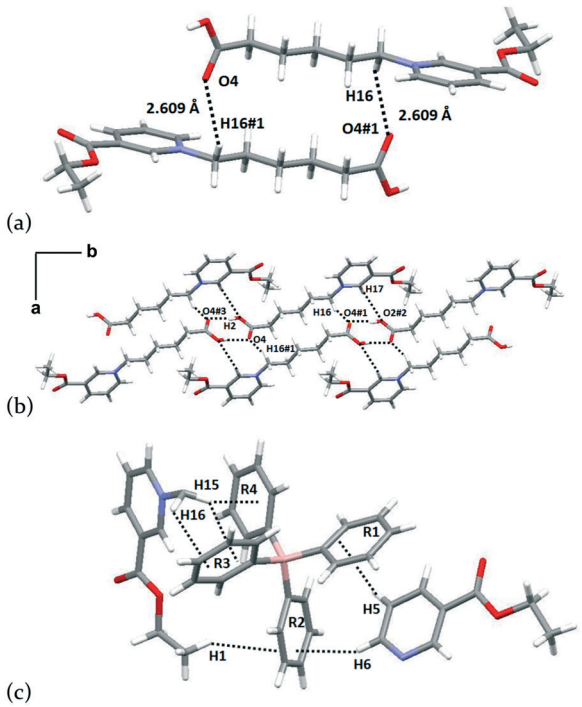

Fig. 2 The hydrogen-bonding motif and packing of the $B(Ph)_4^-$ salt (**2**). (a) The rectangular building block. (b) The 1-D belt structure layer stacking with cations. (c) The formation of the C–H…π interactions between cations and anion.

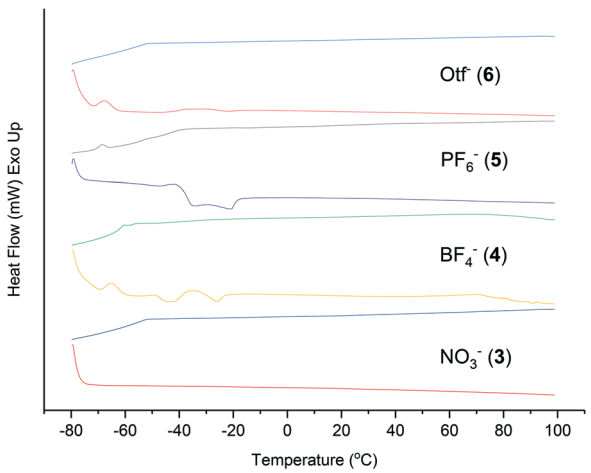

Fig. 3 The DSC thermogram for the NO_3^- (**3**), BF_4^- (**4**), PF_6^- (**5**), and OTf^- (**6**) ILs in the temperature range from 193 K to 373 K at a cooling and heating rate of 10 °C min^{-1}.

are liquid at room temperature. The difference between the hydrogen bonding acceptor abilities of the anions (NO_3^-, BF_4^-, PF_6^- and OTf^-) and carbonyl O atoms (carboxylic acid and ester groups) are small, hence, the disturbance effect of the rotatable ethoxyl groups is enhanced which enables the conformation of the ethoxyl nicotinate cations and the packing to become more flexible and variable, resulting in a liquid state.

Thermal analysis

Thermal analysis of the four ILs, NO_3^- (3), BF_4^- (4), PF_6^- (5), and OTf^- (6), was carried out by means of differential scanning calorimetry at a temperature range of 193 K to 373 K. Fig. 3 shows a thermogram for the four ILs at a cooling and heating rate of 10 °C min^{-1}. In the cooling cycle, the onset glass transition temperatures (T_g) for NO_3^- (3), BF_4^- (4), PF_6^- (5), and OTf^- (6) are −52, −61, −39 and −50 °C, respectively. However, in the heating cycle, cold crystallization (T_{cc}) and melting temperatures (T_m) were observed for BF_4^- (4) (T_{cc} = −66 and T_m = −43, −26 °C), PF_6^- (5) (T_{cc} = −41 and T_m = −35, 21 °C), and OTf^- (6) (T_{cc} = −67 and T_m = −22 °C). The ionic compounds are characterized as ILs by the presence of typical T_g, T_{cc} and T_m thermal behaviours.[24]

IR spectra

In this work, the IR spectra of the solid state Br^- (1) and $B(Ph)_4^-$ (2) as well as the ILs NO_3^- (3), BF_4^- (4), PF_6^- (5) and OTf^- (6) are shown in Fig. 4. The stretching frequency

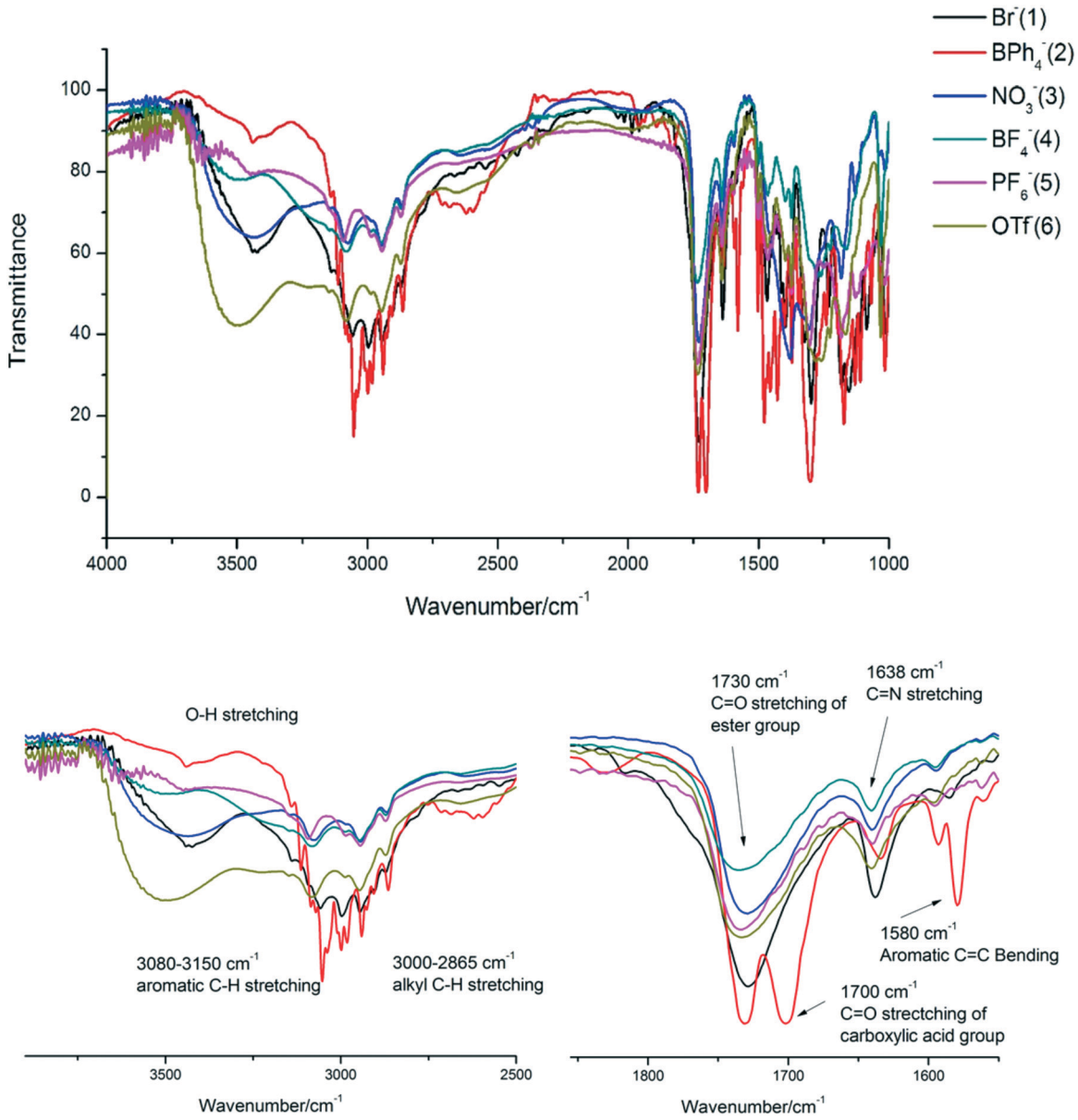

Fig. 4 FTIR spectra of Br^- (1), $B(Ph)_4^-$ (2), NO_3^- (3), BF_4^- (4), PF_6^- (5), and OTf^- (6) ionic compounds.

assignments for ILs 3–6 can then be used to identify the hydrogen bonding patterns based on the IR spectra of the solid-state Br^- (1) and $B(Ph)_4^-$ (2) salts in which the stretching frequencies could correlate to the related hydrogen bonding motifs observed in the crystal structures. Acid hydroxyl stretching frequencies appear in the range of 3700 and 3160 cm^{-1}. As shown in Fig. 4(b), the Br^- (1) and two ILs NO_3^- (3) and OTf^- (6) have strong and broad bands, however the $B(Ph)_4^-$ (2) and two ILs BF_4^- (4) and PF_6^- (5) have relatively weak bands. We suggest that the acid hydroxyl groups of NO_3^- (3) and OTf^- (6) are bonded to the anion to form a C(═O)OH…O_{anion} hydrogen bonding like that present in the Br^- (1) salt. However, the carboxylic acid groups of the ILs BF_4^- (4) and PF_6^- (5) form a cyclic carboxylic acid dimer motif like that in the $B(Ph)_4^-$ (2) salt. The aromatic and alkyl C–H stretching frequencies appear in the ranges of 3150–3080 and 3000–2865 cm^{-1},[25] respectively. One stretching frequency around 2980 cm^{-1} related to CH_3 stretching can only be found for Br^- (1) and $B(Ph)_4^-$ (2) salts in solid but not for the other four ILS. We suggest that this result is caused by the ethoxyl groups which are fixed in salts 1 and 2 but free rotated in ILs 3–6. Additionally, the broad peaks show the mixing of the carbonyl stretching frequency of the ester and carbonyl acid groups at 1730 cm^{-1} for all the ionic compounds except for the $B(Ph)_4^-$ (2) salt. For $B(Ph)_4^-$ (2),[25] the broad peak is split into two signals at 1730 and 1700 cm^{-1} because of the formation of the dimeric carboxylic acid, as shown in Fig. 2b. The C═N stretching and C═C bending frequencies for all six ionic compounds were observed at around 1640 and 1580 cm^{-1}.

Ionic conductivity of ILs

The ionic conductivity of ILs 3–6 was measured to evaluate their potential application as electrolytes. Esters are flexible functional groups due to the rotating C–O–C bonds and tend to be less rigid and have a lower melting point for the formation of ILs. The ionic conduction results for 1-(5-carboxypentyl)-3-(ethoxycarbonyl)pyridin-1-ium ionic compounds with the different anions NO_3^- (3), BF_4^- (4), PF_6^- (5), and OTf^- (6) were measured using comb-shaped gold electrodes. The conductivities were measured in the direction of ion transport along the glass surface.[26–28]

The data listed in Table 1 show that ionic conductivity follows the trend of $BF_4^- > PF_6^- > NO_3^- > OTf^-$ for the same 1-(5-carboxypentyl)-3-(ethoxycarbonyl)pyridin-1-ium cation. The best ionic conductivity of 2.283×10^{-2} Scm^{-1} was obtained for BF_4^- (4). Generally, this ionic conductivity is relatively low[29] compared with the conventional organic electrolyte $LiPF_6$ which has an ionic conductivity of $\sim 10^{-2}$ Scm^{-1} for.[30] This small anion has higher mobility in ionic conductivity[28] and is expected to show faster diffusion, with a decreasing trend upon increase in the size of the anion and the interionic interactions. There are many factors that commonly affect the transport properties for ionic conductivity, such as cation and anion sizes,[28] electrical charge density,[31] temperature,[31] viscosity,[32] and molecular interactions[32] (*e.g.*, interionic hydrogen bonds). There are two perspectives of ionic anions that can be used to explain these ionic conductivity results. One is that a smaller and lighter anion has a high ionic conductivity[33] because it can easily move in a fluid. The other is that interionic hydrogen bonds form against the movement of the anion. In this case, the BF_4^- presents the highest ionic conductivity of the anions examined because the BF_4^- anion is not only small in size but also has the weakest hydrogen bonds compared to the other ILs. Moreover, Table 1shows that the ionic conductivity of the PF_6^- anion is 3.3235×10^{-3} Scm^{-1}. The PF_6^- anion is slightly larger and exhibits slower mobility than the BF_4^- anion. Following the same trend, both NO_3^- and OTf^- anions have larger sizes and stronger interionic hydrogen bonding than BF_4^- and PF_6^{-1},[34] thus they have lower ionic conductivities of 1.6908×10^{-5} and 1.6062×10^{-5} Scm^{-1}, respectively.

Table 1 Ionic conductivity at room temperature of ionic liquids

Anion	NO_3^- (3)	BF_4^- (4)	PF_6^- (5)	OTf^- (6)
σ (Scm^{-1})	1.6908×10^{-5}	0.0228	3.3235×10^{-3}	1.6062×10^{-5}

Measured by impedance measurement.

Conclusions

Here, we report a series of fatty acid-substituted ethylnicotinate ionic compounds with the anions Br^- (1), $B(Ph)_4^-$ (2), NO_3^- (3), BF_4^- (4), PF_6^- (5), and OTf^- (6). The cations of the two crystal structures of Br^- (1) and $B(Ph)_4^-$ (2) form dimerized secondary rectangular motifs with weak C–H…O═C hydrogen bonds and construct a lipid-like bilayer and β-sheet like tape structures, respectively. For the other four ionic compounds, NO_3^- (3), BF_4^- (4), PF_6^- (5), and OTf^- (6), the ester motif disturbs the molecular stacking, reducing the melting point and causing the formation of ionic liquids. This result highlights the effects of the hydrogen bonding acceptor ability of anions and two carbonyl O atoms (acid and ester) of Nia-OEt-C5COOH cation, and the flexible ester group on the melting point of the six ionic compounds. We also hope the results will help in the design of supramolecular architectures and low ionic conductivity ILs.

Conflicts of interest

There are no conflicts to declare.

Acknowledgements

The work was supported by the Ministry of Science and Technology (MOST) of Taiwan (MOST-103-2113-M-017-005-MY3) and National Kaohsiung Normal University. The authors would like to thank Ms Pei-Lin Chen (National Tsing Hua University) for single-crystal X-ray structure determinations.

References

1 H. Jiang, P. Hu, J. Ye, K. K. Zhang, Y. Long, W. Hu and C. Kloc, *J. Mater. Chem. C*, 2018, **6**, 1884.
2 C. B. Aakeröy and A. S. Sinha, *Co-crystals: Preparation, Characterization and Applications*, Royal Society of Chemistry, 2018.
3 E. L. Krueger, A. S. Sinha, J. Despera and C. B. Aakeröy, *CrystEngComm*, 2017, **19**, 4605–4614.
4 H. L. B. Boström, M. S. Senn and A. L. Goodwin, *Nat. Commun.*, 2018, **9**, 2380.
5 D. Braga, F. Grepioni, L. Maini and S. d'Agostino, *Eur. J. Inorg. Chem.*, 2018, **32**, 3597–3605.
6 K. Goossens, K. Lava, C. W. Bielawski and K. Binnemans, *Chem. Rev.*, 2016, **116**, 4643–4807.
7 A. S. Hanamertani, R. M. Pilus, N. A. Manan, S. Ahmed and M. Awang, *Energy Fuels*, 2018, **32**, 6545–6556.
8 T. J. D. Souza Ramos, G. H. Berton, T. M. M. Cassol and S. A. Júnior, *J. Mater. Chem. C*, 2018, **6**, 6270–6279.
9 M. Suckow, M. Roy, K. Sahre, L. Häußler, N. Singha, B. Voit and F. Böhme, *Polymer*, 2017, **111**, 123–129.
10 M. Watanabe, M. L. Thomas, S. Zhang, K. Ueno, T. Yasuda and K. Dokko, *Chem. Rev.*, 2017, **117**, 7190–7239.
11 S. Hisamitsu, N. Yanai and N. Kimizuka, *Angew. Chem., Int. Ed.*, 2015, **54**, 11550–11554.
12 D. Wang, H. Wang and H. Li, *ACS Appl. Mater. Interfaces*, 2013, **5**, 6268–6275.
13 K. S. Egorova, E. G. Gordeev and V. P. Ananikov, *Chem. Rev.*, 2017, **117**, 7132–7189.
14 L. Zerkoune, S. Lesieur, J.-L. Putaux, L. Choisnard de, A. Gèze de, D. Wouessidjewe de, B. Angelov, C. Vebert-Nardin, J. Doutch and A. Angelova, *Soft Matter*, 2016, **12**, 7539–7550.
15 Y. Chen, A. Angelova, B. Angelov, M. Drechsler, V. M. Garamus, R. Willumeit-Römere and A. Zou, *J. Mater. Chem. B*, 2015, **3**, 7734–7744.
16 A. Angelova, B. Angelov, R. Mutafchieva, S. Lesieur and P. Couvreur, *Acc. Chem. Res.*, 2011, **44**, 147–156.
17 P. Y. S. Su, C.-J. Chang and K. M. Lee, *CrystEngComm*, 2016, **18**, 7516–7522.
18 A. S. Amarasekara, *Chem. Rev.*, 2016, **116**, 6133–6183, and references therein.
19 G. Sheldrick, *Acta Crystallogr., Sect. A: Found. Crystallogr.*, 2008, **64**, 112–122.
20 T. Ohtake, M. Ogasawara, K. Ito-Akita, N. Nishina, S. Ujiie, H. Ohno and T. Kato, *Chem. Mater.*, 2000, **12**, 782–789.
21 J. C. W. Tseng, R. Rondla, P. Y. S. Su and I. J. B. Lin, *RSC Adv.*, 2013, **3**, 25151–25158.
22 A. K. Wu and K. M. Lee, *CrystEngComm*, 2012, **14**, 3424–3432.
23 W. L. Li, A. K. Wu and K. M. Lee, *CrystEngComm*, 2012, **14**, 6072–6078.
24 D. R. MacFarlane, M. Kar and J. M. Pringle, *Fundamentals of Ionic Liquids: From Chemistry to Applications*, Wiley-VCH, Weinheim, 2017.
25 Y. Wu, S. Jiang and Y. Ozaki, *Spectrochim. Acta, Part A*, 2004, **60**, 1931–1939.
26 M. Yoshio, T. Mukai, K. Kanie, M. Yoshizawa, H. Ohno and T. Kato, *Adv. Mater.*, 2002, **14**, 351–354.
27 P. Y. S. Su, J. C. W. Tseng, K. M. Lee, J. C. Wang and I. J. B. Lin, *Inorg. Chem.*, 2014, **53**, 5902–5910.
28 P. Y. S. Su, S. J. Hsu, J. C. W. Tseng, H. F. Hsu, W. J. Wang and I. J. B. Lin, *Chem. – Eur. J.*, 2016, **22**, 323–330.
29 M. Watanabe, M. L. Thomas, S. Zhang, K. Ueno, T. Yasuda and K. Dokko, *Chem. Rev.*, 2017, **117**, 7190–7239.
30 K. Xu, *Chem. Rev.*, 2004, **104**, 4303–4418.
31 J. Vila, L. M. Varela and O. Cabeza, *Electrochim. Acta*, 2007, **52**, 7413–7417.
32 H. Takeuchi, T. Ichikawa, M. Yoshio, T. Kato and H. Ohno, *Chem. Commun.*, 2016, **52**, 13861–13864.
33 I. Bandrés, D. F. Montaño, I. Gascón, P. Cea and C. Lafuente, *Electrochim. Acta*, 2010, **55**, 2252–2257.
34 K. Fumino, S. Reimann and R. Ludwig, *Phys. Chem. Chem. Phys.*, 2014, **16**, 21903–21929.